Chapter

Use of Hybrid Methods (Hole-Drilling and Ring-Core) for the Analysis of the RS on Welded Joints

Bernardo Zuccarello

Abstract

The hybrid methods (HMs) for the residual stress (RS) analysis, such as the well-known hole-drilling method (HDM) and the ring-core method (RCM), have been widely developed since 80'. They are mechanical methods based on the partial relaxation of the RSs that occur when a proper geometry variation of the analysed component is introduced by drilling a hole (HDM) or a proper annular groove (RCM). The RS computation is performed by measuring the strains relaxed on surface and then by combine properly such measured strains with the influence coefficients previously computed accurately by using a numerical codes that consider the geometry of the particular component to be examined. In such a manner, the HMs can be potentially applied to any RS distribution independently from the cause that have caused them. In more detail, the HMs can be used for the analysis of the RS on welded joint by using both classical welding methods, as MIG or TIG processes, or modern methods as friction stir welding, etc. In the present chapter, after a brief presentation of the theory of the HMs, their application to various cases of welding joints are treated, and the possible limitation are discussed.

Keywords: residual stresses, hybrid methods, hole-drilling method, ring-core method

1. Introduction

The Hole Drilling Method (HDM) and the Ring-Core Method (RCM) are semi-destructive mechanical method widely used for the residual stress (RS) evaluation in mechanical components [1–12]. Each of two methods have a proper application field; respect to the more known HDM, the RCM is characterized by a higher stress relaxation that allows the user to extend the RS analysis up to about 5÷7 mm from the surface of the analysed component, whereas the HDM allows to analyse the RS up to about 1.5–2 mm. Although several applications have been performed in the various industrial fields along with a lot of research works for both the methods, the RCM has never been considered by standardization organisms, whereas the HDM has been standardised by the ASTM since the 80′. In practice, for both the methods, the most

accurate computational approach used for the evaluation of a generic non-uniform RS distribution, is the so called Integral Equation Method proposed by Schajer (HDM) [6, 7] and Ajovalasit et al. (RCM) [13]; such computational approaches has been included in the ASTM E837-13a standard [14]. However, the very different geometrical variation introduced by the RCM (annular groove) and the HDM (simple hole) involve the presence of different influence parameters on the the RS analysis. In the past the HDM has been used more widely than the RCM thank to its lower damaging and easier experimental procedure. However, the use of the RCM is increased in recent years, especially in Europe, also thank to new modern equipment commercially available [15]. The diffusion of both the methods is corroborated by the high number of special strain gauge rosettes sold in the world by the most famous strain gauge manufacturer as the American MM or the Germany HBM. Also, both the method attract again various research activities having the aim to improve the accuracy of such methods, see as an example the works devoted to the error and uncertainty analysis [16, 17], recently reported in literature.

2. Procedure for the RS evaluation by the HMs

In general the application of the HMs (HDM and RCM) consist on:

1. installation of a special rectangular rosette (see **Figures 1** and **2**) on the surface of the component to be examined;

2. execution of a proper geometry variation (annular groove or hole) by n successive depth increments Δz_i (i = 1,2 ... .n);

3. measuring the three relaxed strains (ε_{ai}, ε_{bi}, ε_{ci}) after each groove depth increment (see an example **Figure 1**);

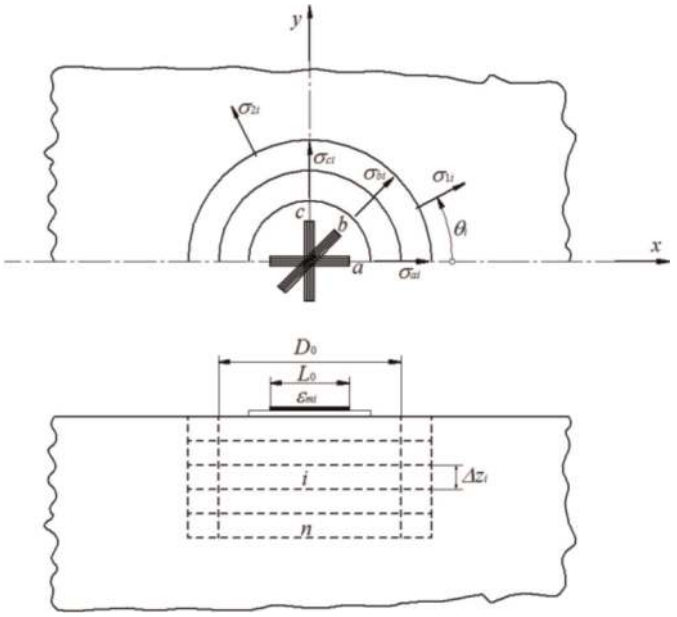

Figure 1.
Ring-Core Method: general notations and groove depth increments.

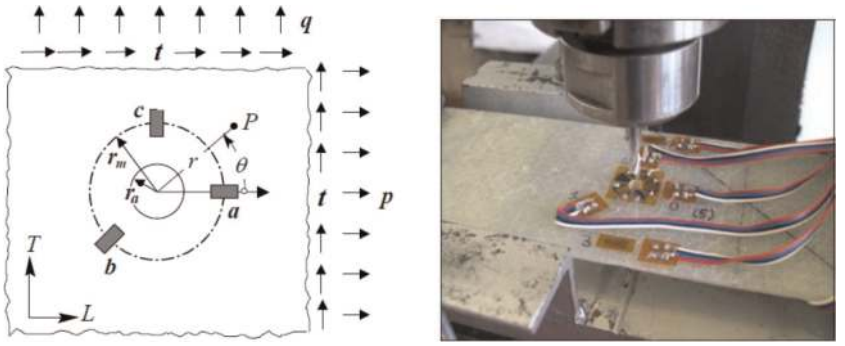

Figure 2.
Typical Experimental setup used by the HDM for the experimental RS analysis.

4. computing the three strain components p_i, q_i, t_i by the simple formulas:

$$p_i = \frac{\varepsilon_{ci} + \varepsilon_{ai}}{2}; \tag{1}$$

$$q_i = \frac{\varepsilon_{ci} - \varepsilon_{ai}}{2} \tag{2}$$

$$t_i = \frac{\varepsilon_{ci} + \varepsilon_{ai} - 2\varepsilon_{bi}}{2} \tag{3}$$

computing the corresponding three stress components P_i, Q_i, T_i ($i = 1,2 \ldots n$) by the iterative relationships (Eqs. 4, 5 and 6):

$$P_i = \frac{1}{a_{ii}}\left[p_i c_E c_\nu - \sum_{j=1}^{i-1} a_{ij} P_j\right] \tag{4}$$

$$Q_i = \frac{1}{b_{ii}}\left[q_i c_E c_\nu - \sum_{j=1}^{i-1} b_{ij} Q_j\right] \tag{5}$$

$$T_i = \frac{1}{b_{ii}}\left[t_i c_E c_\nu - \sum_{j=1}^{i-1} b_{ij} T_j\right] \tag{6}$$

where a_{ij} and b_{ij} ($i = 1,2 \ldots n$, $j = 1,2 \ldots i$) are the well known influence coefficients obtained by proper numerical simulations [6, 7, 14], whereas c_E and c_ν represent the elastic corrective coefficients for the actual material characteristics (E,υ) of the examined component, that are equal to E/E_0 and $(1 + \nu_0)/(1 + \nu)$ respectively, being E_o and υ_o the material characteristics used in the numerical simulations.

Computing the principal residual stresses $\sigma_{1i,2i}$ ($i = 1,2 \ldots n$) and the relative orientation θ_i ($i = 1,2 \ldots n$) as (Eqs. 7 and 8):

$$\sigma_{1i,2i} = P_i \pm \sqrt{Q_i^2 + T_i^2}; \tag{7}$$

$$\theta_i = \frac{1}{2}\arctan\left(\frac{-T_i}{Q_i}\right) \tag{8}$$

In the following **Figure 1** the experimental setup of the RCM is depicted, along with the relative general notations.

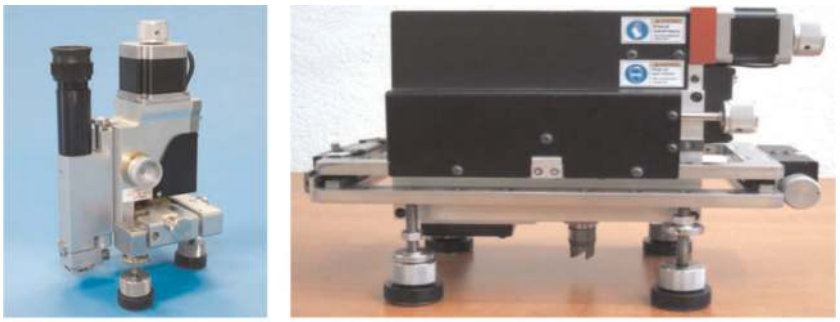

Figure 3.
Modern equipment used for the RS analysis by the HDM (a) and RCM (b).

It is note that the experimental setup of the HDM differs from that of that of the RCM (compare **Figures 1** and **2**) simply for the different rosette used, a special rosette with separate grids that allows to drill a centered hole for a HDM, instead a stacked rosette that allows to minimize the dimension of the groove as well as to avoid the electrical disconnection of the rosette during the successive execution of the depth increments, performed by an annular cutter.

Recently the application of the HMs is performed by using automatic systems that use high speed drilling methods (obtained by proper miniaturized air turbines) and accurate centering systems that involve optical microscopes and step-by-step electric motors. As an example **Figure 3a** shows a diffuse system used for the practical application of the HDM, whereas **Figure 3b** shows a similar system used for the RCM.

It is important to note that the use of such modern systems allows the user to realize the hole or the groove by limiting significantly the further RS introduced by machining (thanks to the high speed machining), as well as center accurately the rosette thanks to the use of the optical microscope and step-by-step electric motors used to move accurately the cutter in the plane parallel to the component surface (see **Figure 3**).

3. Accurate evaluation of the influence coefficient by numerical methods

For the correct computation of the RS by using the HMs, an accurate evaluation of the influence coefficient a_{ij} and b_{ij} ($i = 1,2 \ldots n, j = 1,2 \ldots i$) involved into Eq. 4–6 is necessary. As above mentioned, such coefficients are determined by using a numerical code (FEM, BEM etc) by considering the step-by step procedure for RS analysis. In detail, according to Eq. 4–6 the generic coefficient a_{ij} ($i = 1,2 \ldots n, j = 1,2 \ldots i$) is determined by considering a numerical model that represent the component to be examined with a uniform hydrostatic stress distribution applied only to the *i-th* depth increment of the geometry variation (hole or annular groove) having j total depth increments. The b_{ij} ($i = 1,2 \ldots n, j = 1,2 \ldots i$) coefficients, instead, can be determined numerically by considering a uniform shear stress distribution [13, 14]. Obviously, fixing the total depth, the accuracy of the in-depth RS profile determined by the HMs, increase with the number of depth increments used to reach the total depth although, as it has been demonstrated in [11, 14] if the depth increments are too small then the solution of the inverse problem represented by Eqs.(4–6), became ill-conditioned and

also small errors in the strain measurements due to various spurious influence parameters lead to significant errors on the computed stresses. For this reason in general the use of about 6–8 non-uniform depth increments are advised by following the rule clear exposed in [11]. As an example, **Table 1** shows the optimum distribution of depth increments for the RCM by using a total steps included between 4 and 14 (from Ref. [14]); it is seen how the optimised depth increments are relatively larger at the first and specially at the last steps, whereas they are smaller at the intermediate steps. Similar optimized depth increments are provided in [11] for the HDM. Also, **Tables 2 and 3** show the relative optimized influence coefficients a_{ij} and b_{ij} for 8 total depth

Steps N.	Δz_1	Δz_2	Δz_3	Δz_4	Δz_5	Δz_6	Δz_7	Δz_8	Δz_9	Δz_{10}	Δz_{11}	Δz_{12}	Δz_{13}	Δz_{14}
4	1.00	0.90	1.00	2.10										
6	0.70	0.60	0.55	0.60	0.80	1.75								
8	0.60	0.45	0.40	0.40	0.45	0.50	0.70	1.50						
10	0.55	0.40	0.35	0.30	0.30	0.35	0.40	0.45	0.65	1.25				
12	0.50	0.30	0.30	0.25	0.25	0.25	0.25	0.30	0.40	0.45	0.60	1.15		
14	0.45	0.30	0.25	0.25	0.25	0.20	0.20	0.25	0.25	0.30	0.30	0.40	0.55	1.05

Table 1.
Optimum distribution of depth increment for RCM with total groove depth of 5 mm.

n=1	.0232							
n=2	.0424	.0284					$-a_{n1}$	
n=3	.0573	.0462	.0288					
n=4	.0686	.0579	.0449	.0265				
n=5	.0766	.0662	.0543	.0403	.0224			
n=6	.0821	.0719	.0604	.0476	.0337	.0176		
n=7	.0878	.0778	.0667	.0547	.0424	.0306	.0284	
n=8	.0897	.0798	.0688	.0571	.0452	.0341	.0396	.0109
	i=1	i=2	i=3	i=4	i=5	i=6	i=7	i=8
n=1	.0214							
n=2	.0385	.0224					$-b_{n1}$	
n=3	.0512	.0395	.0237					
n=4	.0658	.0554	.0414	.0217				
n=5	.0785	.0668	.0543	.0409	.0174			
n=6	.0892	.0777	.0652	.0505	.0358	.0124		
n=7	.1093	.0959	.0813	.0663	.0514	.0360	.0179	
n=8	.1198	.1066	.0920	.0760	.0605	.0451	.0478	.0106

Table 2.
Influence coefficients relative to a thick component (>100 mm) with standard dimension of the core-rosette assembly (Do=14 mm, Lo = 5 mm).

n=1	.0190							
n=2	.0372	.0246					$-a_{n1}$	
n=3	.0517	.0415	.0257					
n=4	.0632	.0534	.0411	.0238				
n=5	.0720	.0622	.0507	.0373	.0203			
n=6	.0782	.0685	.0574	.0449	.0315	.0161		
n=7	.0854	.0757	.0648	.0529	.0410	.0294	.0265	
n=8	.0883	.0785	.0677	.0560	.0443	.0333	.0383	.0102
	i=1	i=2	i=3	i=4	i=5	i=6	i=7	i=8
n=1	.0170							
n=2	.0335	.0186					$-b_{n1}$	
n=3	.0488	.0369	.0192					
n=4	.0620	.0523	.0403	.0175				
n=5	.0744	.0646	.0528	.0396	.0149			
n=6	.0862	.0755	.0633	.0495	.0348	.0104		
n=7	.1062	.0942	.0806	.0659	.0510	.0354	.0177	
n=8	.1190	.1059	.0913	.0755	.0598	.0449	.0475	.0094

Table 3.
Influence coefficients relative to a thin component (<15 mm) with standard dimension of the core-rosette assembly (Do =14 mm, Lo = 5 mm).

increments, with refer to a thick (**Table 2**) and a thin component analysed by the RCM (**Table 3**).

Although for standard dimensions of the geometry variation properly introduced by the HDM, the relative influence coefficients are provided by the same ASTM standard [13], and similarly accurate evaluation of the coefficients for the RCM are provided in [14], in particular practical cases where the analysed component cannot be considered as an infinite plate subjected to a plane stress field, the relative influence coefficient have to be determined by specific numerical simulations, that consider the exact geometry of the component to be examined. As occur in many inverse problems, the evaluation of the RS from the strains relaxed on surface after each depth increment is influenced by several influence parameters that can introduce into the evaluated RS a significant uncertainty, so that an accurate RS evaluation needs to a reliable estimation of the corresponding uncertainty. For this reason, interesting study are reported in literature that deal with the evaluation of the accuracy and of the uncertainty that affect the principal RS computed by using both the HDM [16] and the RCM [17]. Such interesting works contain the formulas that the user can use to an accurate estimation of the uncertainty of the RS after the analysis and the correction of the main influence parameters, as the thermal effects due to machining, the zero depth offset, the rosette eccentricity, the stresses induced by machining and so on. Synthetically, such studies have been demonstrated that using modern apparatus as that shown in **Figure 3**, in good experimental conditions the uncertainty of the principal RS computed by the RCM in general falls in the range 10–55 MPa [17]

moving from the first to the last steps; similarly for the HDM the mean uncertainty is in general equal to about ±25 MPa [16].

4. Application of the HDM for the analysis of the RS in a welded joint

As above mentioned, the HMs can be advantageously applied for the RS analysis in welded joints between metal components. As an example, in the following the use of the HDM for the RS analysis on a I type welded joint between two stainless steel plates (AISI 304) is exposed in detail, and the results are compared with that computed numerically by using a FEM procedure accurately accomplished by using accurate thermal analysis of the welding process considered as a progressive process constituted by successive welding passes [18].

Figure 4 show the geometry of the joint considered and the relative FE model used for the RS analysis, accomplished by considering that the weld bead is formed by 5 successive passes that are simulated by changing the material properties according the temperature profile relieved experimentally by proper thermocouples installed near the weld bead.

The distribution of the RS along the y direction, computed by the numerical simulation process implemented, is reported in **Figure 5**. As expected, it is seen how

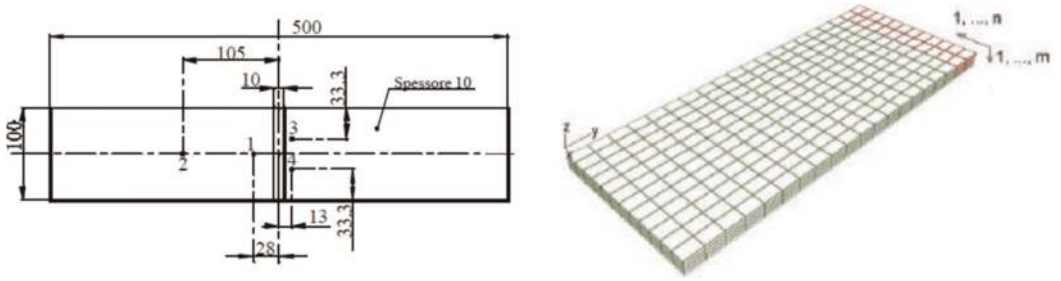

Figure 4.
Geometry of the welded butt joint considered (a) and relative FE model used for the numerical simulation of the welding process.

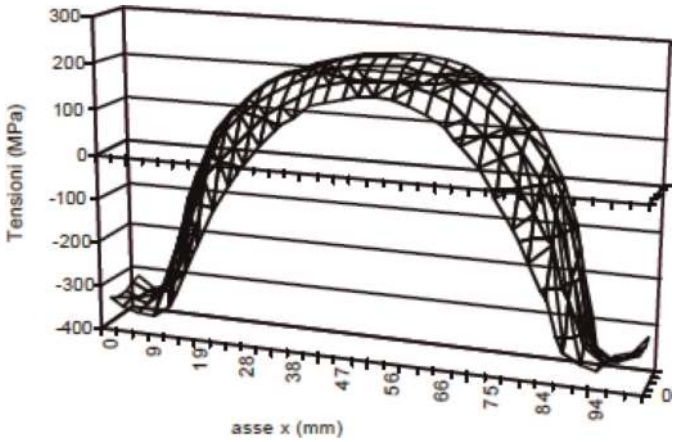

Figure 5.
Distribution of the RS along y direction (σy) computed by accurate FE simulations.

the maximum RS occur at the central zone of the weld bead, with values that fall in the range 200–205 MPa (about 60% the material yield stress).

From **Figure 5** it is seen how the RS vary significantly along the x direction, whereas they vary lightly in the y direction. For this reason the comparison between the RS computed numerically and that estimated experimentally by the HDM is carried out by considering the points 3 and 4 in **Figure 4**, i.e. by considering point near the weld bead in which the geometry of the surface is not significantly modified by the welding process. In detail, the following **Figures 6** and **7** show the comparison between the in-depth RS profile computed by numerical simulations and the RS distribution near the surface computed by using the HDM. The analysis of such figures show how the profile computed numerically is always inside the uncertainty range of the RS computed by means of the HDM, corroborating the accuracy of such an experimental method.

5. Analysis of through-thickness RS in aluminium FSW butt joints

The HMs can be also used for the analysis of the through-thickness RS in friction stir welding on metals. As an example in [19] the HDM have been advantageously used for the analysis of the RS in FSW butt joints between plate made by aluminium. In detail, using the HDM the in-depth RS distribution in the zone close to the tool shoulder border of the joint advancing side, has been accurately determined by considering also different aluminium alloys (AA1050 O, AA2024 T4, AA6982 T6, AA7075

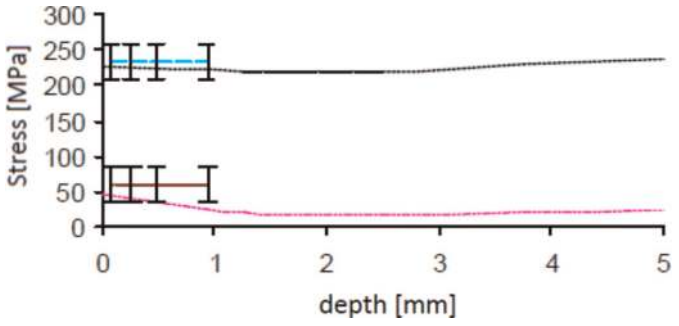

Figure 6.
*Comparison between the RS computed by the HDM in point 3 of **Figure 4** and the RS profile obtained by accurate numerical simulations.*

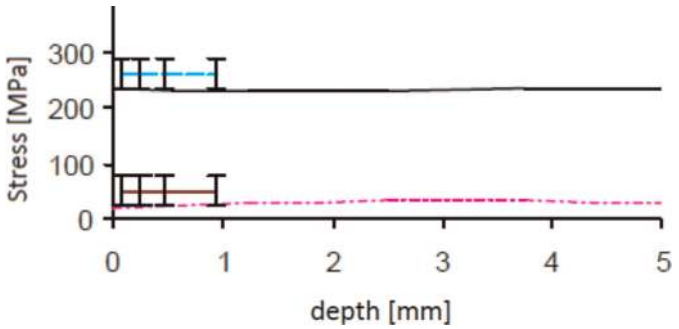

Figure 7.
*Comparison between the RS computed by the HDM in point 4 of **Figure 4** and the RS profile obtained by accurate numerical simulations.*

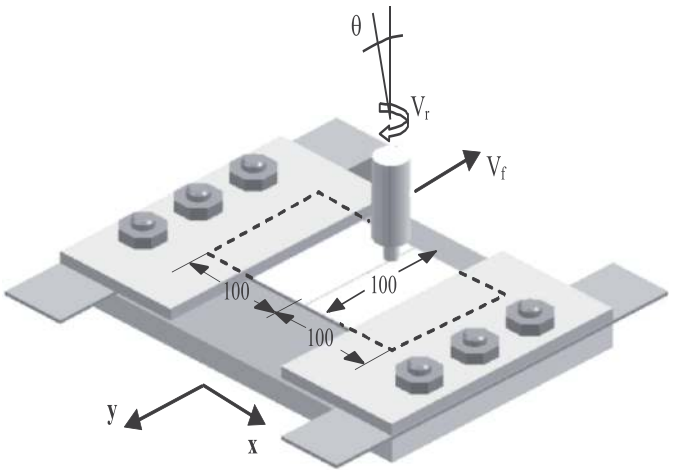

Figure 8.
Sketch of the FSW butt joint considered, during the welding process.

T6) and different specific thermal contribution (STC) that characterizes the velocity of the welding process. **Figure 8** shows the sketch of the FSW butt joint considered, during the welding process.

In detail, it is considered the case in which the FSW of a butt joint is obtained by inserting a specially designed pin, rotating with velocity V_r into the adjoining edges of the sheets to be welded, and then moving it all along the joint with velocity V_f (**Figure 8**). The realization of the weld bead leads to significant changes of the mechanical properties and of the microstructure of the material near the weld bead. In detail, as it shown in **Figure 9**, it is possible to distinguish the following areas:

a. Parent material, i.e. the remote material that is not subjected to the heat flux and conserves the original mechanical properties and microstructure;

b. Heat affect Zone (HAZ), i.e., the material subjected to a thermal cycle with a consequent microstructure and mechanical properties modification, although without any plastic deformations;

c. Thermo-Mechanical Affect Zone (TMAZ), i.e. the zone where the material is subjected to plastic deformation and significant heat flux with consequent variations of the mechanical properties and of the microstructure (no recrystallization phenomena);

d. Nugget, i.e. the recrystallized area in which the original grains are replaced with fine and equiaxed recrystallized grains with nominal dimensions of few micrometers.

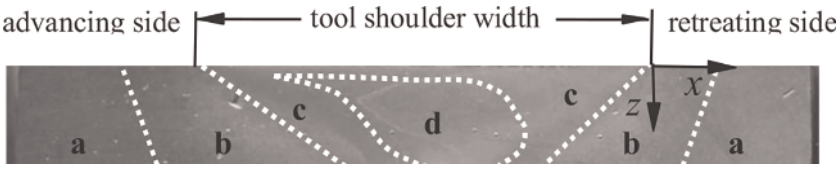

Figure 9.
Material microstructures in a typical transversal section of an aluminium AA6082-T6 FSW butt joint.

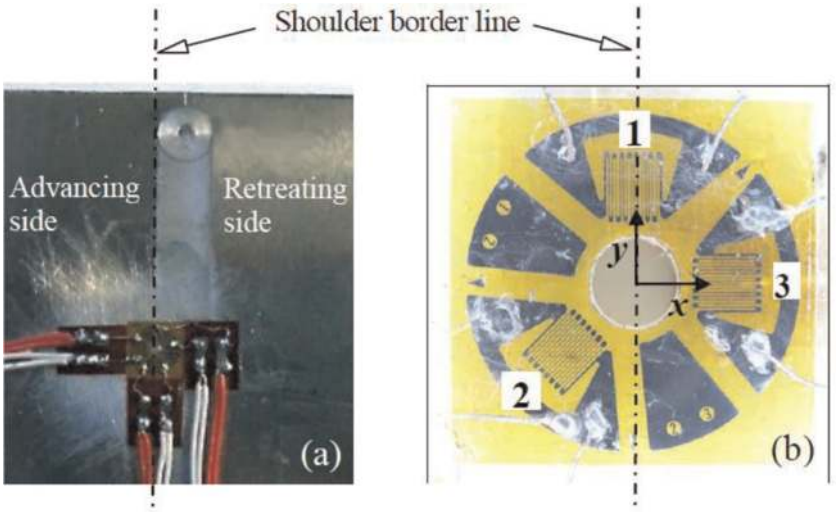

Figure 10.
(a) Rosette installation on a welding specimen and (b) details of the rosette.

In order to analyse the most relevant residual stress distribution that occur through the thickness of the welding joint, a special rectangular strain gauge rosette type MM EA-062RE-120, have been bonded into the welded specimens, with the 1 grid aligned with the tool shoulder border of the joint advancing side (see **Figure 10**), that is the zone of the welding seam where the maximum values of the RS are expected [19].

After the strain gauge rosette installation, it has been linked to a proper multichannel strain gauge monitoring machine (HBM UPM 100), and the three strains relaxed after each successive increase of the hole depth, have been collected by using a software [20] properly developed by the maker of the milling machine shown in **Figure 3**. In detail, such an advanced machine have an high speed air turbine and a special microscope, that permit respectively to limit the residual stresses due to machining as well as the rosette eccentricity. Also, the hole has been drilled by 25 successive steps of 0.1 mm (total hole depth of 2.5 mm), by using a tungsten carbide mill. In accordance with the ASTM standard [14], as well as with the good practice indications reported in Refs. [11, 12, 16], the measuring procedure have been performed in such a way to minimize the spurious residual stress induced by the hole drilling.

5.1 Residual Stress evaluation

The evaluations of the residual stresses through the thickness of the examined welded bead, have been carried out by using the calculation process exposed in chapter 2, and the discrete results have been fitted with simple polynomial functions. Then, it permits to perform the uniformity test prescribed by the ASTM standard [14] and then to compute uniform or non-uniform residual stresses by the Integral Method exposed in detail in the previous chapter 2. As an example, considering the case of the aluminum AA1050-O FSW joints with medium specific thermal contribution (MSTC), **Figure 11** shows the typical curves of the three relaxed strains (ε_1, ε_2, ε_3).

From **Figure 11** it is seen how, the surface relaxed strains take initially typical negative values due to the relaxation of positive RS; successively they increase in

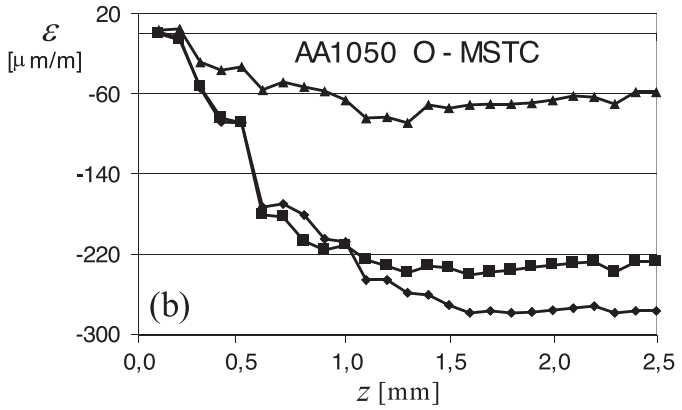

Figure 11.
Typical relaxed strain curves relative to AA1050-O aluminum joints, with MSTC.

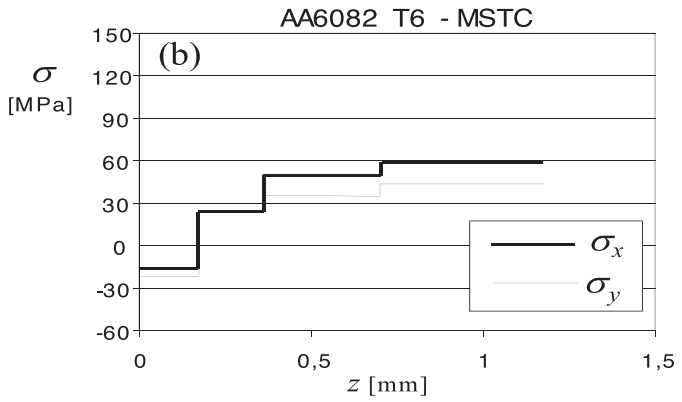

Figure 12.
Typical residual stresses relative to AA6082-T6 joints, with MSTC.

module (up to 140 to 280 μm/m) until hole depth of 1.5–2.0 mm, at which they take a flat trend (saturation of the surface relaxation phenomenon). Similar relaxation curves have been acquired for all the aluminium alloys considered and for all the manufacturing conditions (STC) studied.

As an example, **Figure 12** shows the RS computed by considering the case of AA6082 T6 FSW joints with medium specific thermal contribution (MSTC). Similar trends have been obtained for the other cases examined.

Figure 12 permits to observe that in all the three examined cases (AA6082 T6, AA1050-O, AA2024-T4), both the main RS components, acting on x and y directions respectively, take similar values and trends (increasing with depth). In detail, they range from negative value (on surface, from −8 MPa to −30 MPa), to positive values of about 60 MPa for MSTC (40 MPa and 90 MPa for LSTC and HSTC respectively) at depth of about 0.5 ÷ 1 mm. Therefore, for this aluminum alloy in the STC examined range (from LSTC to HSTC) the maximum stresses decrease if the STC value increase. Very interesting is the comparison of RS evaluated for the different materials and for the three different STC levels considered, which shows that unlike the traditional welded joints, in the examined FSW butt joints, the maximum RS do not occur on joint surface but inner to the weld at a depth from surface that varies from 0.5 to 1.25 mm. In more detail, for the aluminum alloys commonly used in the structural design (AA6082 T6 and AA2024-T4) the surface residual stress σ_s takes in practice

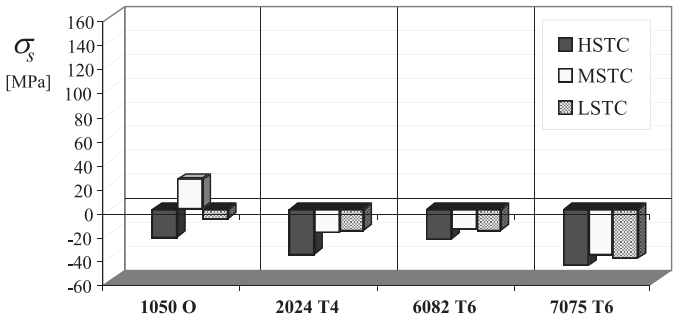

Figure 13.
Residual stresses measured on surface of the FSW joints.

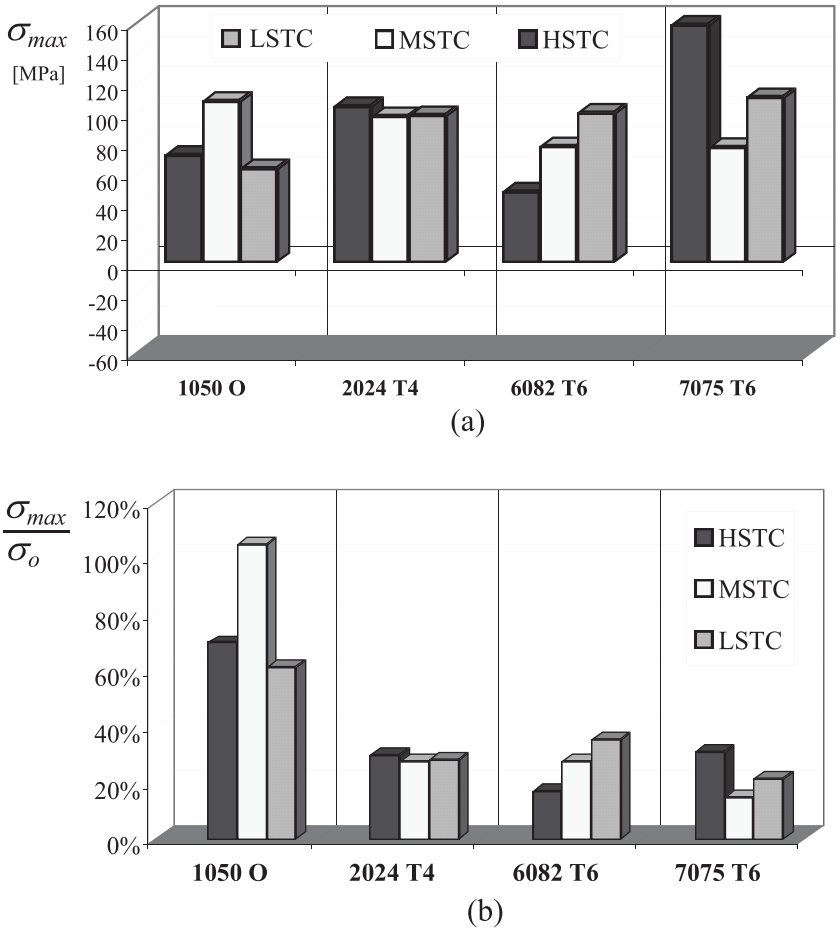

Figure 14.
Maximum residual stresses measured along the thickness of the joints: (a) absolute values and (b) percentage of the parent material yield stress value.

always negative values ranging from −20 to −40 MPa (see **Figure 13**), i.e. it takes always values less than 20% of the yielding stress σ_o.

Additionally, the HDM has allowed to highlight that the maximum residual stresses σ_{max} varies from about 50 to 150 MPa (see **Figure 14a**), i.e. from about 15–30% the yielding stress, depending to the particular material type and the STC level (see **Figure 14b**).

Finally, it is important to note that if the use of the HMs leads to significant plasticity effects at the bottom of the geometry variation (hole or groove) due to high RS levels, than values of the principal RS computed by the above exposed procedure should be corrected by using the procedure reported in literature [21, 22], to which the reader is addressed.

6. Conclusions

The above reported applications of the HDM show that in principle the HMs methods can be advantageously used for the experimental RS analysis in welded joints. As above mentioned the HDM allows to detect the RS until depth of about 1.5–2 mm under the component surface, whereas the RCM allows to reach depths until 4–5 mm. In detail, the accurate use of such methods need the use of modern systems equipped with a high speed machining cutter to minimize the RS due to machining, and a proper microscope to minimize the rosette eccentricity error. The main limitation of the HMs are related to the possible surface curvature of the welded bead and to the particular geometry of the joint. Obviously, in case of non-plane surface and non-plane welded components, the influence coefficients should be computed properly by specific and accurate numerical simulations. In general, to limit the experimental work it is convenient to apply the HMs directly into the zone where other independent considerations (as coarse numerical simulation or theoretical consideration s etc.)

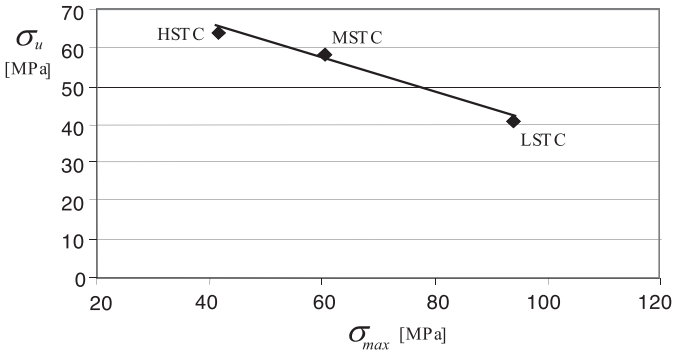

Figure 15.
Ultimate tensile stress of AA6082-T6 joints, with HSTC, MSTC and LSTC.

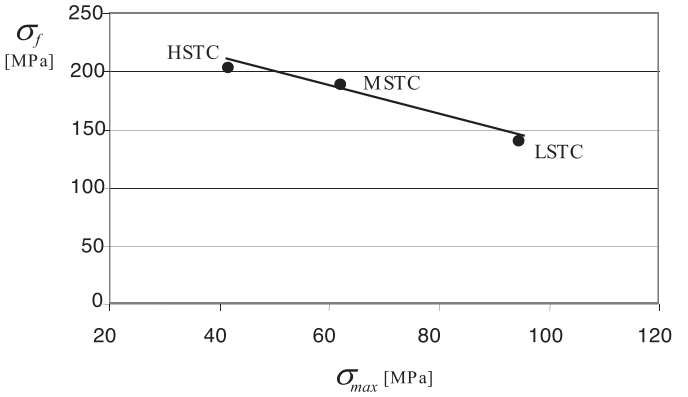

Figure 16.
Fatigue strength of AA6082-T6 joints, welded with HSTC, MSTC and LSTC.

indicate as the more stressed zone. As an example, as above clearly shown, in case of a butt joint the more stressed zone coincides with the zone near the central point, whereas in case of FSW butt joint the more stressed point is that close to the tool shoulder border in the advancing side of the joint. In such a manner the use of a unique experiment allow**s** the user to evaluate the maximum residual stress that influence not only the static strength but also the fatigue strength of the welded joint. As an example **Figures 15 and 16** shows the correlation between the maximum RS (σ_{max}) computed by applying the HDM and the static (**Figure 15**) and the fatigue (**Figure 16**) strength of an AA6082 – T6 FSW butt joint, varying the STC.

It is seen a linear relationship between the maximum RS (σ_{max}) and the mechanical strength. Such a linear relationship is in accordance with the Goodman criterion commonly used in the mechanical design to estimate the mean stress effect on the metal fatigue resistance. Moreover, the generic good accordance relieved in the above exposed application (as in many other application here not mentioned for brevity sake), permits to establish that the HMs, widely employed in the industrial field due to its simplicity and low cost, allows the user an accurate estimation of the maximum residual stresses that occur in an a generic welded joint realized by traditional techniques (TIG, MIG etc.) or by innovative techniques (friction stir welding etc). Obviously, in general the HMs can be advantageously used to optimize the parameters that govern the welding process in order to minimize the maximum RSs and, consequently, the mechanical properties of the examined welded joint.

Author details

Bernardo Zuccarello
Dipartimento dell'Innovazione Industriale e Digitale (DIID), Università di Palermo, Palermo, Italy

*Address all correspondence to: bernardo.zuccarello@unipa.it

References

[1] Kelsey RA. Measuring non-uniform residual stresses using the hole-drilling method. Proceedings of the Society for Experimental Stress Analysis. 1956;**14**: 181-194

[2] Nickola WE. Practical subsurface residual stress evaluation by the hole-drilling method. In: Proceedings of the 1986 SEM Spring Conference. 1986. pp. 47-58

[3] Bijak-Zochoski MA. Semi destructive Method of Measuring Residual Stresses. VDI-Beritche. 1978;**313**:469-476

[4] Niku-Lari A, Lu J, Flavonet JF. Measurement of Residual Stress Variation with Depth by the Hole Drilling Method. Experimental Mechanics. 1985;**25**:175-185

[5] Flaman MT, Manning BH. Determination of the Residual Stress Variation whith Depth by the Hole Drilling Method. Experimental Mechanics. 1985;**25**:205-207

[6] Schajer GS. Measurement of non-uniform residual stresses using the hole-drilling method Part. I and II. Journal of Materials Engineering Technology. 1988; **110**(4):338-343

[7] Zuccarello B. Analisi delle Tensioni Residue con il Metodo della Cava Anulare. Cosenza: Proceedings of the XXIII Aias National Conference; 1994. pp. 87-91

[8] Zuccarello B. Optimization of Depth Increment Distribution in the Ring-Core Method. Journal of Strain Analysis for Engineering Design. 1996;**31**(4):251-258

[9] Schajer GS. Non-uniform Residual Stresses Measurement by the Hole-drilling Method. Strain. 1992;**28**(2):19-22

[10] Petrucci G, Zuccarello B. A New calculation procedure for non-uniform residual stress analysis by the hole drilling method. Journal of Strain Analysis. 1988;**33**(1):27-37

[11] Zuccarello B. Optimal calculation steps for the evaluation of residual stress by the incremental hole-drilling method. Experimental Mechanics. 1999;**39**(2): 117-124

[12] Schajer GS, Altus E. Stress calculation error analysis for incremental hole drilling residual method. Journal of Engineering Materials and Technology. 1996;**118**(1):120-126

[13] Ajovalasit A, Petrucci G, Zuccarello B. Determination of Non-uniform Residual Stresses Using the Ring-Core Method. Transactions of the ASME - Journal of Engineering Materials and Technology. 1996;**118**(2):224-228

[14] ASTM. Standard test method for determining residual stresses by the hole-drilling strain gauge method. In: International Designation E 837-13a, United States. 2013. p. 16

[15] VALENTINI E, BENINCASA A, BERTELLI L. An automatic system for measuring residual stresses by Ring-core method, Italian Stress Analysis Association, 40th National Congress. Palermo, Italy: University of Palermo; 2011

[16] Scafidi M, Valentini E, Zuccarello B. Error and Uncertainty Analysis of the Residual Stresses Computed by Using the Hole Drilling Method. Strain. 2011; **47**(4):301-312

[17] Zuccarello B. Error and uncertainty analysis of non-uniform residual stress evaluation by using the ring-core

method. Experimental Mechanics. 2016; **56**(9):20-35

[18] Cappello F, Carlisi G, Zuccarello B. Valutazione Numerica e Verifica Sperimentale dello Stato Tensionale in una Giunzione Saldata di Testa. In: Proceedings of the XXXI National Aias Conference. 2002. pp. 18-21

[19] Fratini L, Zuccarello B. An analysis of through-thickness residual stresses in aluminium FSW butt joints. International Journal of Machine Tools and Manufacture. 2006;**46**:611-619

[20] Valentini E. An automatic System for Measuring Non –Uniform Residual Stress by the Hole Drilling Method. Turin: XIII IMEKO World Congress; 1997. pp. 5-9

[21] Petrucci G, Zuccarello B. Effect of plasticity on the residual stress measurement using the groove method. Strain. 1996;**32**:97-104

[22] Beghini M, Bertini L, Raffaelli P. An account of the plasticity in the hole drilling method for residual stress measurement. Journal of Strain Analysis. 1994;**30**:227-233